

## Article

# Artificial Neural Network Modeling to Predict Thermal and Electrical Performances of Batteries with Direct Oil Cooling

Kunal Sandip Garud <sup>1</sup>, Jeong-Woo Han <sup>2</sup>, Seong-Guk Hwang <sup>1</sup> and Moo-Yeon Lee <sup>1,\*</sup> 

<sup>1</sup> Department of Mechanical Engineering, Dong-A University, 37 Nakdong-Daero 550, Saha-gu, Busan 49315, Republic of Korea; 1876936@donga.ac.kr (K.S.G.); 2178735@donga.ac.kr (S.-G.H.)

<sup>2</sup> Thermal Management R&D Center, Korean Automotive Technology Institute, 303 Pungse-ro, Pungse-Myun, Cheonan 31214, Republic of Korea; jwhan1@katech.re.kr

\* Correspondence: mylee@dau.ac.kr; Tel.: +82-51-200-7642

**Abstract:** The limitations of existing commercial indirect liquid cooling have drawn attention to direct liquid cooling for battery thermal management in next-generation electric vehicles. To commercialize direct liquid cooling for battery thermal management, an extensive database reflecting performance and operating parameters needs to be established. The development of prediction models could generate this reference database to design an effective cooling system with the least experimental effort. In the present work, artificial neural network (ANN) modeling is demonstrated to predict the thermal and electrical performances of batteries with direct oil cooling based on various operating conditions. The experiments are conducted on an 18650 battery module with direct oil cooling to generate the learning data for the development of neural network models. The neural network models are developed considering oil temperature, oil flow rate, and discharge rate as the input operating conditions and maximum temperature, temperature difference, heat transfer coefficient, and voltage as the output thermal and electrical performances. The proposed neural network models comprise two algorithms, the Levenberg–Marquardt (LM) training variant with the Tangential-Sigmoidal (Tan-Sig) transfer function and that with the Logarithmic-Sigmoidal (Log-Sig) transfer function. The ANN\_LM-Tan algorithm with a structure of 3-10-10-4 shows accurate prediction of thermal and electrical performances under all operating conditions compared to the ANN\_LM-Log algorithm with the same structure. The maximum prediction errors for the ANN\_LM-Tan and ANN\_LM-Log algorithms are restricted within  $\pm 0.97\%$  and  $\pm 4.81\%$ , respectively, considering all input and output parameters. The ANN\_LM-Tan algorithm is suggested to accurately predict the thermal and electrical performances of batteries with direct oil cooling based on a maximum determination coefficient ( $R^2$ ) and variance coefficient (COV) of 0.99 and 1.65, respectively.

**Keywords:** artificial neural network; battery; direct oil cooling; electrical performance; electric vehicle; thermal performance



**Citation:** Garud, K.S.; Han, J.-W.; Hwang, S.-G.; Lee, M.-Y. Artificial Neural Network Modeling to Predict Thermal and Electrical Performances of Batteries with Direct Oil Cooling. *Batteries* **2023**, *9*, 559. <https://doi.org/10.3390/batteries9110559>

Academic Editor: Carlos Ziebert

Received: 11 October 2023

Revised: 13 November 2023

Accepted: 14 November 2023

Published: 16 November 2023



**Copyright:** © 2023 by the authors. Licensee MDPI, Basel, Switzerland. This article is an open access article distributed under the terms and conditions of the Creative Commons Attribution (CC BY) license (<https://creativecommons.org/licenses/by/4.0/>).

## 1. Introduction

The excessive consumption of fossil fuels by internal combustion engine vehicles is causing a rapid increase in greenhouse gas emissions, including environmental contaminants of carbon dioxide (CO<sub>2</sub>), carbon monoxide (CO), nitrogen oxides (NOx), sulfur dioxide (SO<sub>2</sub>), and particulate matter (PM) [1]. To assure a low carbon future, the governments of various countries have passed regulations on emissions, for example, the United States has issued the “1990 Clean Air Act”, European countries have implemented the “Low Emission Zone Program”, and Japan has recirculated the “2007 NOx and PM Law” [2]. Furthermore, the European Commission has introduced the package “Fit for 55” to reduce greenhouse gas emissions up to 55% by 2030 [3]. In global greenhouse gas emissions, the transportation sector is the second largest contributor [4]. Therefore, the current transportation sector is undergoing a drastic change of replacing internal combustion engine vehicles

with electric vehicles to achieve a carbon-free and energy-sustainable future [5,6]. Electric vehicles offer several benefits, such as a safe and clean environment and improved safety and human health [7,8]. In addition, the ecological benefits of electric vehicles could be extended by charging their batteries from renewable energy sources [9].

Electric vehicles are provided with batteries as the main energy storage system on board the vehicle, the energy densities of which are continuously increasing to improve the performance of electric vehicles [10,11]. The battery temperature should be maintained within a range of 20 °C to 45 °C to ensure safe and efficient operations [12,13]. However, the increasing energy densities result in higher heat generation, thus degrading the performance and operational life of batteries [14]. Furthermore, the excessive heat generation during high charging/discharging operations results in thermal runaway and explosion in batteries [15,16]. Therefore, an advanced cooling technique should enable effective thermal management of batteries, which could improve their efficiency and life span and thus the safety and performance of electric vehicles.

Air cooling and indirect liquid cooling are commercially adopted for the thermal management of electric vehicle batteries [17]. The cooling performance of air cooling is poor and indirect liquid cooling imposes high thermal resistance owing to the existence of cooling channels/plates, which reduces its cooling performance for high power density batteries [18,19]. To overcome the limitations of the existing cooling strategies, research has been initiated to find next-generation thermal management techniques for batteries. Direct liquid cooling diminishes the thermal resistance by enabling direct contact between batteries and the dielectric cooling fluid, hence improving the cooling performance [20,21]. In the last few years, numerous research studies have reported on direct liquid cooling as an emerging battery thermal management technique. Li et al. restricted the temperature of 18650 batteries within 34 °C and 34.5 °C at 4C and 7C discharge rates, respectively, using SF33 coolant-based direct liquid cooling [22]. Patil et al. employed immersion cooling to maintain the maximum temperature of a battery pack within 28 °C at a 3C discharge rate and 10 L/min flow rate [23]. Sundin et al. proposed single-phase immersion cooling, which maintained the battery temperature within 30 °C at a 2C discharge rate, and Zhou et al. further demonstrated that the thermal runaway of batteries was suppressed using two-phase immersion cooling [24,25]. Dubey et al. showed improvements in maximum temperature and pumping power for 21700 batteries with Novec 7500-based direct cooling compared to that with water/glycol-based indirect cooling [26].

In recent years, machine learning is gaining popularity to predict and optimize the performance of physical systems based on various influential variables compared to other prediction approaches. Furthermore, ANN models are widely adopted to replicate the behaviors of specific systems/devices under several conditions owing to the benefits of faster response, minimal error, and least complex mathematical manipulation [27,28]. Numerous studies have confirmed the potential of neural network models to accurately predict the performance of batteries. Panchal et al. proposed a neural network model to predict the thermal and electrical characteristics of batteries under real driving conditions [29]. Furthermore, Wang et al. also predicted the thermal and electrical characteristics of lithium-ion batteries using a coupled thermal-equivalent circuit model integrated with a neural network [30]. Feng et al. predicted the voltage and temperature of batteries using a neural network model under several conditions of current and temperature [31]. Xie et al. developed a back-propagation-based neural network model to estimate battery internal resistance and battery temperature [32]. Arora et al. proposed a neural network model with battery heat generation as the output parameter and battery nominal capacity as the input parameter [33]. Liu et al. developed an ANN model with the structure of 1-30-1 to predict the surface temperature of batteries and pressure drop [34]. Jalilianabar et al. predicted the battery temperature for input conditions of phase change material with and without paraffin/graphene composite, phase change material thickness, time, and discharge rate using a neural network model with an accuracy of 0.99 and mean square error of 0.0173 [35].

The open literature reveals that significant research has reported on direct liquid cooling for next-generation battery thermal management. However, the reported research is not sufficient to commercialize direct liquid cooling and there is scope to extend the research to prove its reliability for battery thermal management. The development of a final-stage direct liquid cooling system for batteries needs extensive efforts in terms of prototype fabrication, testing, and optimization, which are time consuming and expensive. In this scenario, accurately trained neural network models could effectively replicate the performance behavior of a cooling system under actual operating conditions with comparatively less effort. However, there is no concrete research that elaborates neural network modeling for batteries with a direct liquid cooling system. Therefore, in the present study, ANN models based on experimental data are developed to predict the thermal and electrical performances of batteries with direct oil cooling. Two combinations of an algorithm, namely ANN\_LM-Tan and ANN\_LM-Log, are developed to predict the maximum temperature, temperature difference, heat transfer coefficient, and voltage, considering operating conditions of oil temperature, oil flow rate, and discharge rate. The ANN model with the best algorithm is suggested to accurately replicate the performance data of batteries with direct oil cooling under several operating conditions.

## 2. Experimental Method

### 2.1. Experimental Set-Up Description

The experimental set-up of the 18650 battery module with direct oil cooling is depicted in Figure 1. The considered batteries are INR18650 MJ1 3.5 Ah, comprising silicone-graphite as the anode material and NMC-811 as the cathode material and outsourced from LG Chem Ltd. (Seoul, South Korea). The battery module is composed of 16 cylindrical cells with a 4-series and 4-parallel configuration. The specifications of the selected battery cells are presented in Table 1. The battery module is contained within an acryl box, which is filled with dielectric thermal oil manufactured by Shell company. The thermophysical properties of the selected dielectric thermal oil are presented in Table 2 [20]. The oil is distributed around the battery cells through inlet and outlet ports, located at the center on opposite faces of the acryl box. Sixteen T-type thermocouples with a range of  $-200\text{ }^{\circ}\text{C}$  to  $400\text{ }^{\circ}\text{C}$  are used to measure the temperature of the battery module. A thermocouple is attached at the center of each battery cell, considering a negligible temperature difference over the battery cell surface. Li et al. observed that there was no significant difference in battery temperature over its various surface locations [22]. Pt-100 temperature sensors with a range of  $0\text{ }^{\circ}\text{C}$  to  $850\text{ }^{\circ}\text{C}$  are provided at the inlet and outlet of the acryl box to measure the temperature of the oil. A peristaltic pump with a range of  $0.4\text{ mL/min}$  to  $2.2\text{ L/min}$  is used to circulate the oil in the acryl box. The heated oil from the battery module is cooled using a 30 L chiller with range of  $-25\text{ }^{\circ}\text{C}$  to  $80\text{ }^{\circ}\text{C}$ . The terminals of the battery module are connected to the 1.2 kW DC electronic loader (TOYTECH TLF1200, Incheon, South Korea) with a voltage range of 1 V to 150 V and current range of 0 A to 240 A. The electronic loader is used to discharge the battery module at constant current mode, considering different discharge rates ranging from 1C to 4C. The battery module is discharged until the voltage is cut off and rested for 2 h. The fully discharged battery module is charged using a DC power supply with a voltage range of 0 V to 30 V and current range of 0 A to 10 A, considering a charging rate of 0.5C. The battery module is charged in constant current mode with 7 A until it reaches 16.8 V, and then the battery module is maintained at constant voltage mode until the current approaches to 0.2 A. The fully charged battery is rested for 2 h. The battery management unit with passive cell balancing is employed. Furthermore, the rest time after full discharging and charging operations ensures cell balancing of the battery module. All measuring devices are connected to a GL840 data logger to monitor and record the data. The temperature and voltage data of the battery module with direct oil cooling are recorded at each second over the discharge period of battery. The temperature difference and heat transfer coefficient are calculated corresponding to the measured data. The measured and calculated data of the battery module with direct oil cooling are evaluated considering

four oil flow rate conditions of 0.4 L/min, 0.6 L/min, 0.8 L/min, and 1.0 L/min, four oil temperature conditions of 15 °C, 20 °C, 30 °C, and 35 °C, and four discharge rates of 1C, 2C, 3C, and 4C. These measured and calculated data under several operating conditions are employed to develop the ANN models. The sample of the experimental data used for neural network modeling is depicted in Figure 2. The experimental set-up is housed within a chamber with temperature and humidity ranges of −30 °C to 60 °C and 30% to 95%, respectively; therefore, the ambient temperature during all experiments is controlled at 25 °C.

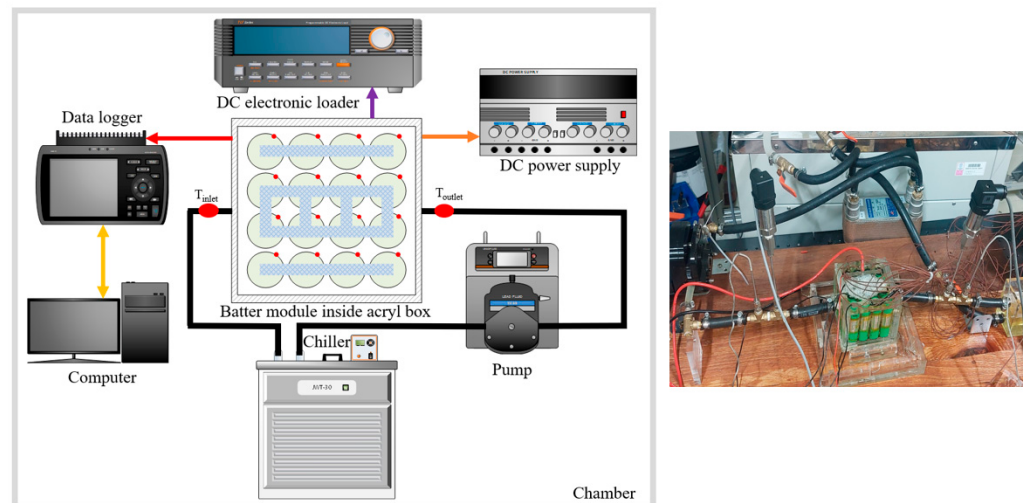


**Figure 1.** Experimental set-up of 18650 battery module with direct oil cooling.

**Table 1.** Specifications of the selected battery cells.

Specification	Value
Nominal capacity (Ah)	3.5
Nominal voltage (V)	3.653
Max voltage (V)	4.2
Discharge cut-off voltage (V)	2.5
Standard charge current (A)	1.7
Standard charge cut-off current (A)	0.050

**Table 2.** Thermophysical properties of dielectric thermal oil.

Property	Value
Density (kg/m <sup>3</sup> )	810
Thermal conductivity (W/m-K)	0.14
Specific heat (J/kg-K)	2100
Viscosity (cSt)	19.4

## 2.2. Experimental Parameters and Uncertainty Analysis

Uncertainty analysis was conducted on the experimental parameters to consider the accuracies of the experimental devices and errors owing to probe position, calibration, and measurement [36,37]. The accuracies labeled with the T-type thermocouples, Pt-100 temperature sensors, DC loader, data logger, and pump were ±0.5%, ±0.25%, ±0.1%, ±0.1%, and ±0.2%, respectively. The uncertainties in various experimental parameters were evaluated using Equation (1) [38]:

$$U_R = \left[ \left( \frac{\partial R}{\partial X_1} U_1 \right)^2 + \left( \frac{\partial R}{\partial X_2} U_2 \right)^2 + \cdots + \left( \frac{\partial R}{\partial X_n} U_n \right)^2 \right]^{\frac{1}{2}} \quad (1)$$

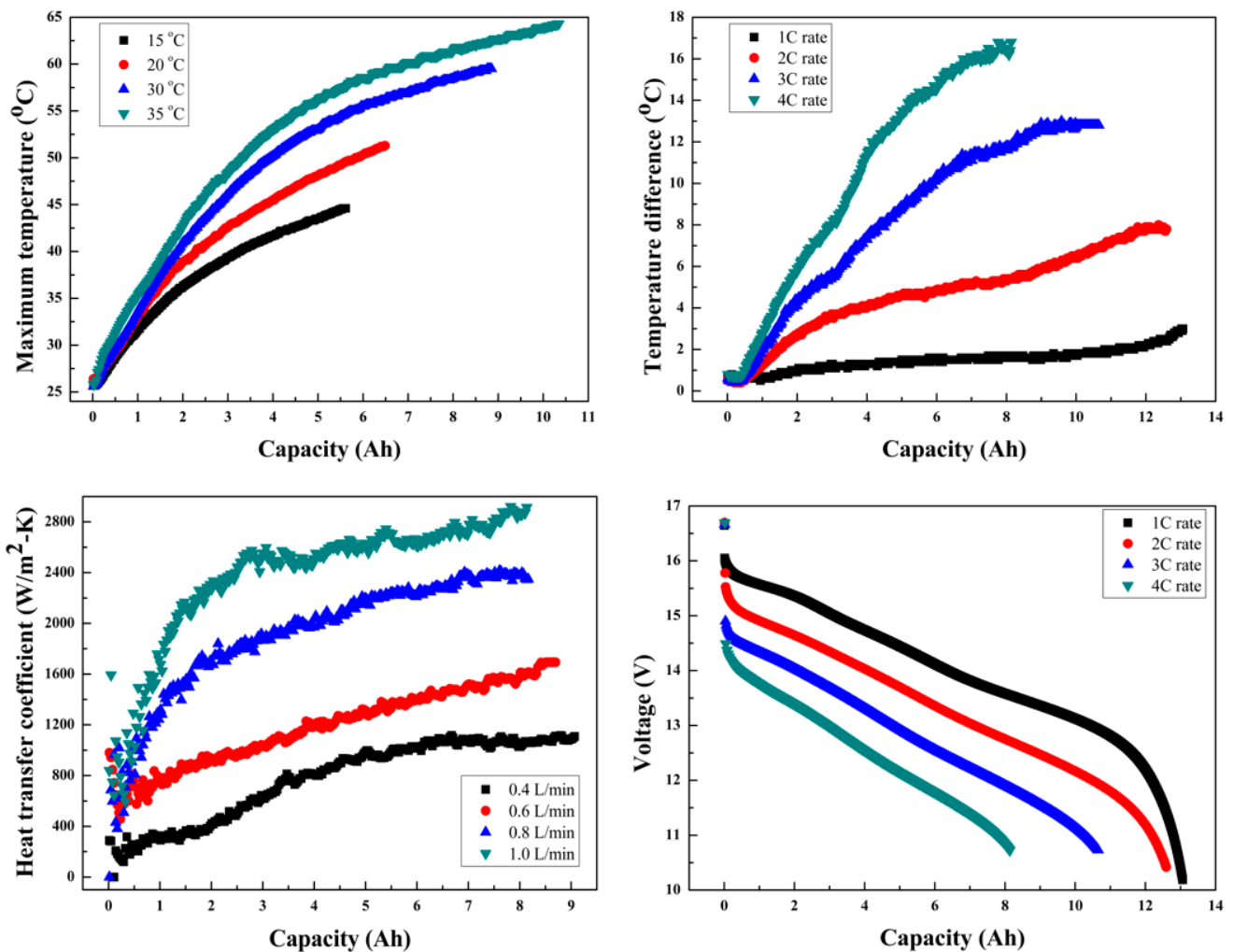


**Figure 2.** Sample of experimental data used for neural network modeling.

Here,  $R$  is the dependent experimental parameter and  $U_R$  is the uncertainty in the dependent experimental parameter, whereas  $X_1, X_2, \dots, X_n$  are independent experimental parameters, and  $U_1, U_2, \dots, U_n$  are the uncertainties in the independent experimental parameters. The uncertainties in measured temperature, voltage, and heat transfer coefficient were evaluated as 3.13%, 1.29%, and 6.45%, respectively.

The temperature difference of the battery module was calculated as follows [39]:

$$\Delta T = T_{max, \text{battery}} - T_{min, \text{battery}} \quad (2)$$

Here,  $T_{max, \text{battery}}$  and  $T_{min, \text{battery}}$  are the maximum and minimum temperatures of the battery module, respectively.

The heat transfer coefficient for the battery module with direct oil cooling was calculated as follows [40]:

$$h = \frac{Q_{convection, \text{oil}}}{A_{battery} \left( T_{mean, \text{battery}} - T_{mean, \text{oil}} \right)} \quad (3)$$

The convective heat transfer from the battery module to the oil was calculated as follows [40]:

$$Q_{convection, \text{oil}} = \dot{m}_{\text{oil}} C_{p, \text{oil}} (T_{outlet, \text{oil}} - T_{inlet, \text{oil}}) \quad (4)$$

Here,  $A_{battery}$  is the surface area of the battery module,  $T_{mean, \text{battery}}$  is the mean temperature of the battery module,  $T_{mean, \text{oil}}$  is the mean temperature of the oil,  $\dot{m}_{\text{oil}}$  is the mass

flow rate of the oil,  $C_{p,oil}$  is the specific heat of the oil, and  $T_{outlet,oil}$  and  $T_{inlet,oil}$  are outlet and inlet temperatures of the oil, respectively.

### 3. Artificial Neural Network Modeling

The non-linear and complex relationship between various performances and influential factors can be effectively mapped with the least computational time using neural network models. The ANN mimics the biological neural structure, which relates larger datasets of various parameters for any physical system [41]. The neural network involves the integration of the neurons in respective layers of input, output and hidden [42]. The input and output parameters decide the number of neurons in respective layers, whereas the numbers of hidden layers and neurons in hidden layers are considered based on the optimized training error [43]. The weights are the connection link between each layer of neurons. Various combinations of algorithms with transfer functions and training variants are employed to train the neural network [44]. The effective mapping pattern between input and output datasets is established by adjusting the weights while neural network training [45].

In the present work, ANN was modeled to predict the thermal and electrical performances of batteries for direct oil cooling considering different operating conditions. The developed ANN model comprised oil temperature, oil flow rate, and battery discharge rate as input neurons in the input layer. And the discharge voltage, maximum temperature, temperature difference, and heat transfer coefficient were included as output neurons in the output layer. The input conditions of oil temperature, oil flow rate, and discharge rate were varied in the ranges of 15 °C to 35 °C, 0.4 L/min to 1.0 L/min, and 1C to 4C, respectively, for neural network modeling. After trying several combinations, the number of hidden layers was adjusted to 2, each with 10 hidden neurons to achieve the minimum error and computational time. Hence, the structure of the proposed ANN model was presented by 3-10-10-4, as depicted in Figure 3. The neural network was trained using a back-propagation algorithm comprising of two combinations of the LM training variant, that with transfer functions of the Tan-Sig and the Log-Sig. MATLAB R2018a software was used for neural network modeling considering the aforementioned parameters and algorithms.

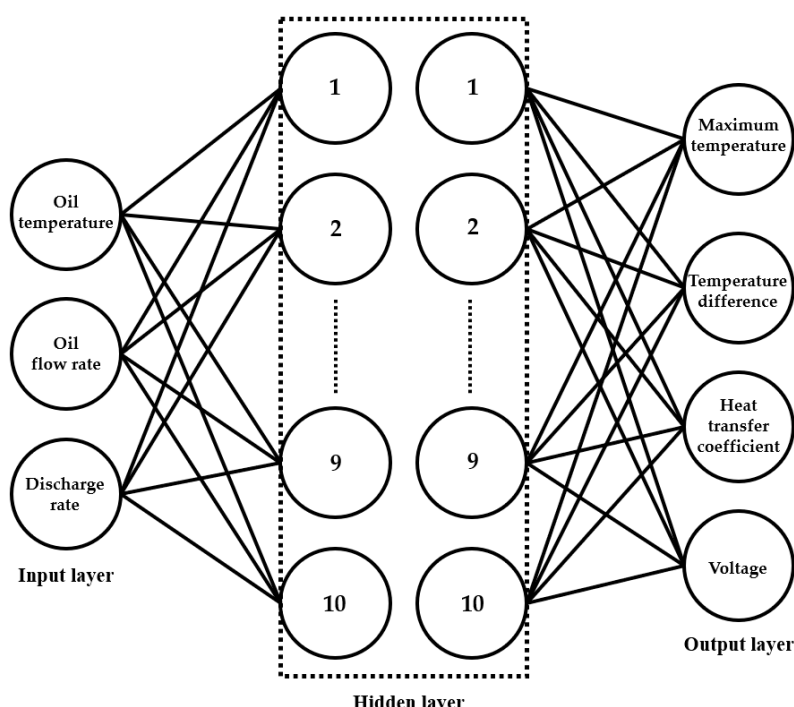


**Figure 3.** Structure of proposed ANN model.

The predicted output from the developed ANN model was expressed as follows [46]:

$$Y^i = G(A^i + U^T Y^{i-1}) \quad (5)$$

Here,  $Y$  is the predicted output,  $G$  indicates the transfer function,  $A$  and  $U$  present the connection and weight matrixes, respectively, and  $i$  stands for the layer number.

The mathematical expressions for the considered Tan-Sig and Log-Sig transfer functions are as follows [41,46]:

$$f(Y) = \frac{1 - e^{-Y}}{1 + e^{-Y}} \quad (6)$$

$$f(Y) = \frac{1}{1 + e^{-Y}} \quad (7)$$

To evaluate the accuracy of the predicted results from the ANN model, three statistical parameters, the coefficient of determination ( $R^2$ ), variance coefficient ( $COV$ ), and mean square error ( $MSE$ ), were calculated using Equations (8)–(10) [47]:

$$R^2 = 1 - \frac{\sum_{i=1}^n (Y_{pre,i} - Y_{mea,i})^2}{\sum_{i=1}^n (Y_{mea,i})^2} \quad (8)$$

$$COV = \frac{\sqrt{\frac{\sum_{i=1}^n (Y_{pre,i} - Y_{mea,i})^2}{n}}}{|\bar{Y}_{mea}|} \times 100 \quad (9)$$

$$MSE = \frac{1}{n} \sum_{i=1}^n (Y_i - \bar{Y})^2 \quad (10)$$

Here,  $Y_{pre,i}$  is the predicted value at  $i$ th data point,  $Y_{mea,i}$  is the measured value at  $i$ th data point,  $\bar{Y}_{mea}$  is the average value of measured data points, and  $n$  indicates the maximum data points.

The experimental data of the considered input and output parameters were evaluated over the discharge period of the batteries at each second. A time series of experimental data was considered to develop the ANN models. The 1000 data points comprising four performances (output parameters) were evaluated corresponding to three operating conditions (input parameters). Thus, the neural network models were developed for input and output parameters comprising 1000 experimental data points. The total dataset of 1000 data points was divided into three subgroup proportions of 60%, 20%, and 20%, corresponding to training, validation, and testing, respectively. Based on the considered data, the deducted training, validation, and testing errors for the developed ANN model with two algorithms are presented in Figure 4. It should be noted that the input parameter values were fixed; however, the output parameter values were predicted in form of time series over the discharge period of the batteries. And from the predicted results in form of time series, the thermal performance was compared at the end of discharge and electrical performance was compared at the same discharge capacity, considering the variations in various influential factors.

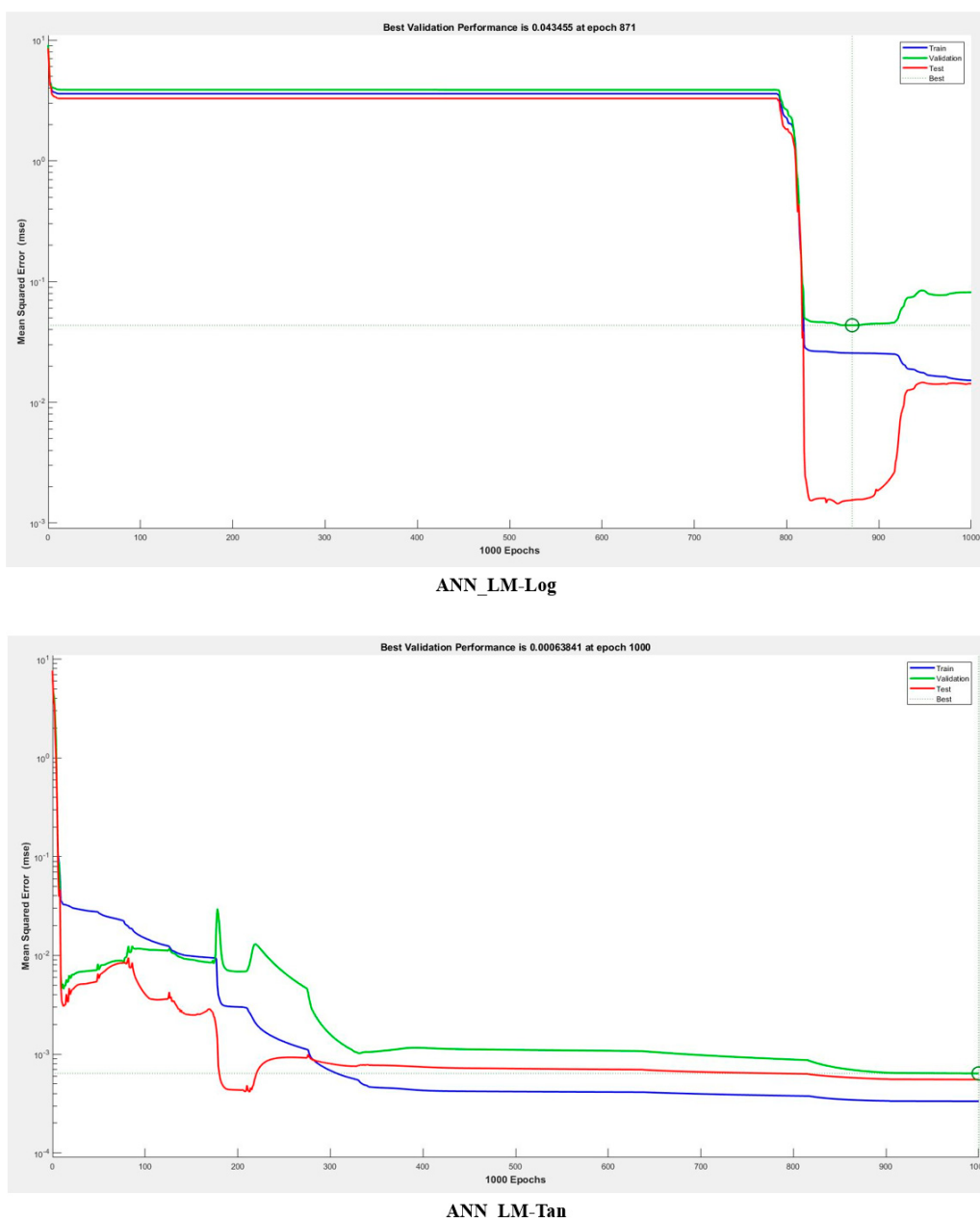


**Figure 4.** Deduced training, validation, and testing errors for developed ANN model with two algorithms.

#### 4. Results and Discussion

The thermal and electrical performances of batteries with direct oil cooling are evaluated and discussed in this section for various operating conditions. Furthermore, the ANN models with two combinations of the algorithm are compared to predict the battery performance under similar operating conditions. The thermal performance under various conditions is elaborated in Section 4.1, followed by Section 4.2 with a discussion of the electrical performance under various conditions, and Section 4.3 presents a replication of the thermal and electric performances by the best ANN algorithm with the experimental results under various discharge capacities.

##### 4.1. Thermal Performance

The maximum temperature, temperature difference, and heat transfer coefficient were evaluated and predicted as the thermal performance of the batteries under various oil temperatures, oil flow rates, and discharge rates. The thermal performance of the batteries

in terms of maximum temperature, temperature difference, and heat transfer coefficient was predicted in form of time series over the discharge period of the batteries, considering variations in oil temperature, oil flow rate, and discharge rate. However, for comparison, the predicted and experimental results of thermal performance at the end of discharge are presented.

#### 4.1.1. Maximum Temperature

The variation in experimental and predicted maximum temperatures of the batteries with change in oil temperature is presented in Figure 5. The difference in temperature between battery and oil decides the rate of dissipated heat generated in the battery. The heat transfer rate is superior when the difference in temperatures between the two sources is high. Therefore, the heat transfer rate from battery module to oil was maximum when oil at a lower temperature contacted the battery surface. The maximum temperature of the batteries increased from  $44.6^{\circ}\text{C}$  to  $64.3^{\circ}\text{C}$  when the oil temperature rose from  $15^{\circ}\text{C}$  to  $35^{\circ}\text{C}$ . Accurate training with lower prediction error in the case of the ANN\_LM-Tan algorithm resulted in closer agreement between predicted and experimental maximum temperatures. The maximum temperature increased from  $44.32^{\circ}\text{C}$  to  $63.76^{\circ}\text{C}$  and  $43.23^{\circ}\text{C}$  to  $61.69^{\circ}\text{C}$  for the ANN\_LM-Tan and ANN\_LM-Log algorithms, respectively, with an increase in the oil temperature from  $15^{\circ}\text{C}$  to  $35^{\circ}\text{C}$ , which indicated corresponding maximum prediction errors of 0.94% and 4.05%.

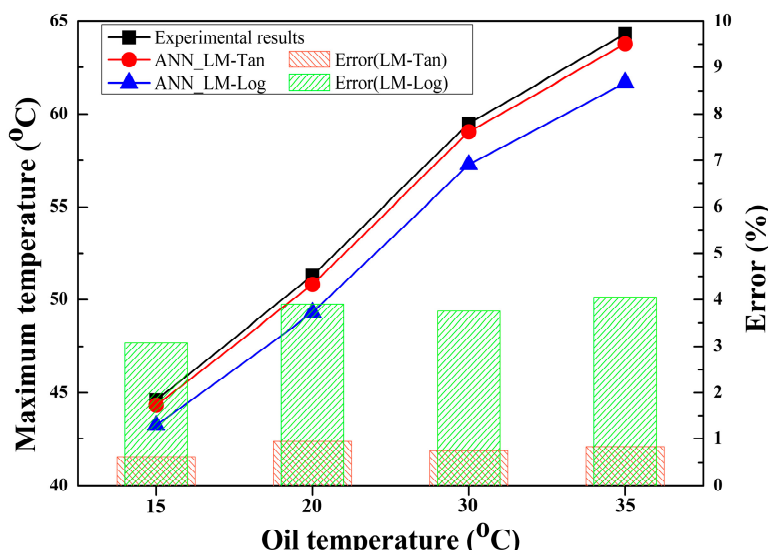


**Figure 5.** Variation in experimental and predicted maximum temperatures of batteries with change in oil temperature.

The experimental and predicted maximum temperatures of the batteries decreased with an increase in oil flow rate, as shown in Figure 6. The convective heat transfer from the battery module to the oil improved as the oil flow rate increased owing to the increase in local obstruction of flowing oil around the battery cells. The predicted maximum temperatures by the ANN\_LM-Tan and ANN\_LM-Log algorithms followed the same trend as the experimental maximum temperature variation with oil flow rate, corresponding to maximum errors of 0.97% and 4.30%. The experimental results and the ANN\_LM-Tan and ANN\_LM-Log algorithms showed decreases in maximum temperature from  $63.40^{\circ}\text{C}$  to  $45.20^{\circ}\text{C}$ ,  $63.91^{\circ}\text{C}$  to  $45.46^{\circ}\text{C}$ , and  $65.73^{\circ}\text{C}$  to  $46.91^{\circ}\text{C}$ , respectively, with an increase in oil flow rate from  $0.4\text{ L/min}$  to  $1.0\text{ L/min}$ .

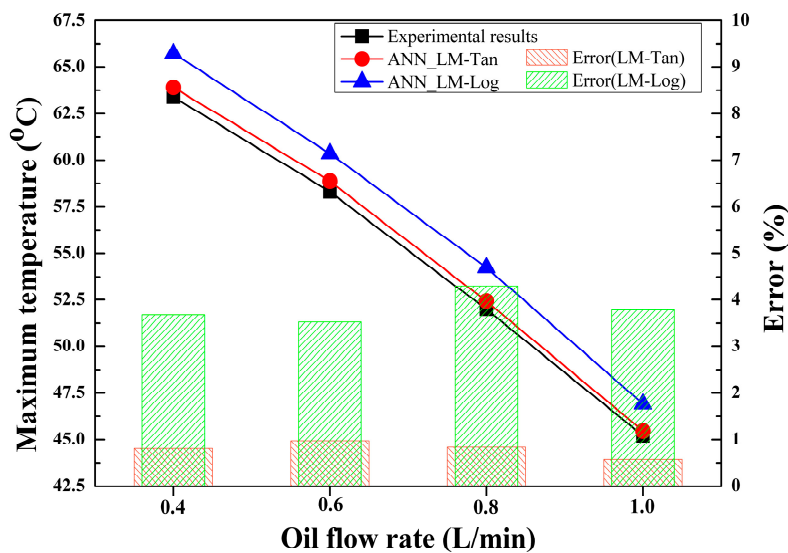


**Figure 6.** Variation in experimental and predicted maximum temperatures of batteries with change in oil flow rate.

The maximum temperature was predicted for the two algorithms and compared with experimental results under various discharge rates, as shown in Figure 7. The batteries generated a larger amount of heat during the high discharge rates; hence, for the same direct oil cooling conditions, the maximum temperature of the batteries increased with an increase in discharge rate. With an increase in discharge rate from 1C to 4C, the experimental results and the ANN\_LM-Tan- and ANN\_LM-Log-predicted maximum temperatures showed increases from 32.40 °C to 60.20 °C, 32.69 °C to 60.68 °C, and 33.51 °C to 62.18 °C, respectively. It can be observed that the predicted maximum temperature by the ANN\_LM-Tan algorithm showed closer agreement with the experimental maximum temperature compared to the ANN\_LM-Log algorithm, with corresponding maximum errors of 0.89% and 4.20%.

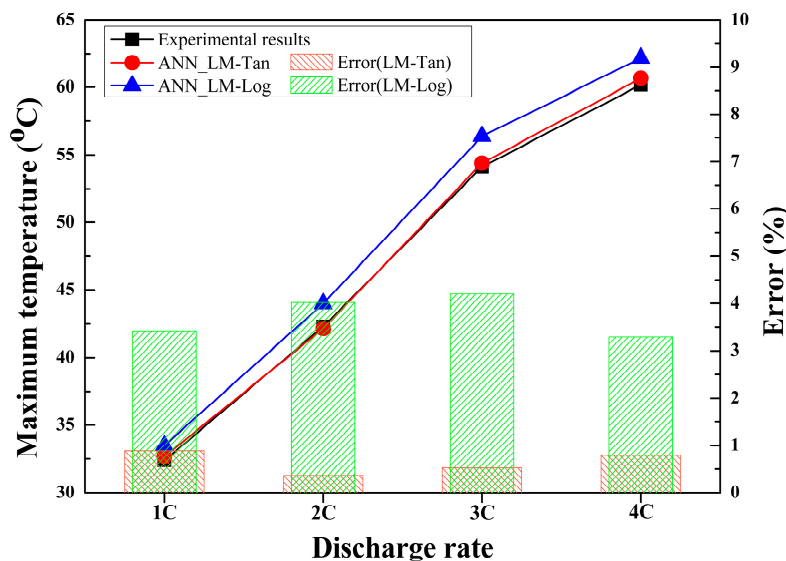


**Figure 7.** Variation in experimental and predicted maximum temperatures of batteries with change in discharge rate.

#### 4.1.2. Temperature Difference

The difference between the maximum and minimum temperatures of the battery module improved with a decrease in oil temperature and increase in oil flow rate. As

explained, the lower oil temperature and high oil flow rate improved the heat transfer rate between battery module and oil, which resulted in a lower temperature difference. In addition, similar to the maximum temperature, the temperature difference also increased as the discharge rate increased owing to an increase in battery heat generation under the same cooling conditions. Figures 8–10 show the variations in experimental and predicted temperature differences with changes in oil temperature, oil flow rate, and discharge rate, respectively. The temperature difference increased from 6.9 °C to 17.3 °C and 3 °C to 16.8 °C with an increase in oil temperature from 15 °C to 35 °C and increase in discharge rate from 1C to 4C, respectively. However, the temperature difference dropped from 16.7 °C to 7.3 °C with an increase in flow rate from 0.4 L/min and 1.0 L/min. In the case of temperature difference, the ANN\_LM-Tan algorithm also had high prediction accuracy with the experimental results compared to the ANN\_LM-Log algorithm for all oil temperatures, oil flow rates, and discharge rates. The maximum errors between the predicted and experimental temperature differences were 0.95% and 4.29% in the case of oil temperature, 0.96% and 4.86% in the case of oil flow rate, and 0.81% and 3.52% in the case of discharge rate, corresponding to the ANN\_LM-Tan and ANN\_LM-Log algorithms, respectively.

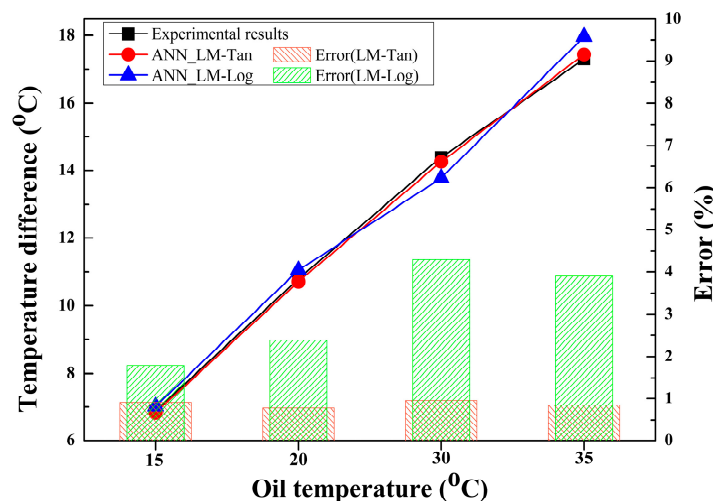


**Figure 8.** Variation in experimental and predicted temperature difference of batteries with change in oil temperature.

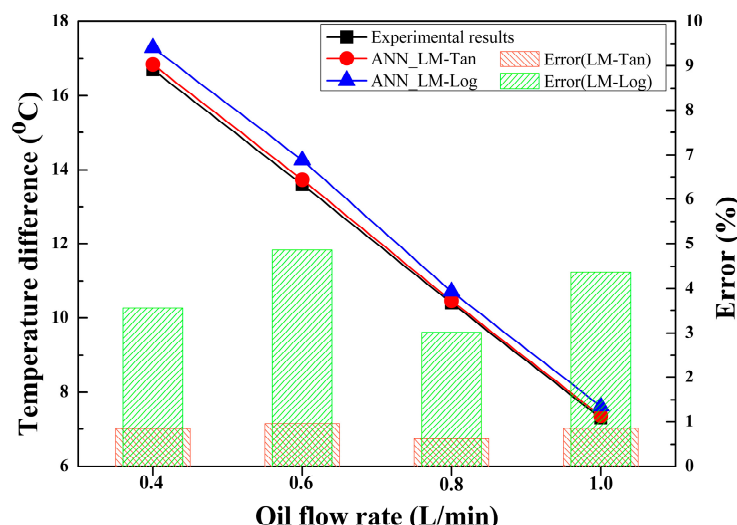


**Figure 9.** Variation in experimental and predicted temperature difference of batteries with change in oil flow rate.

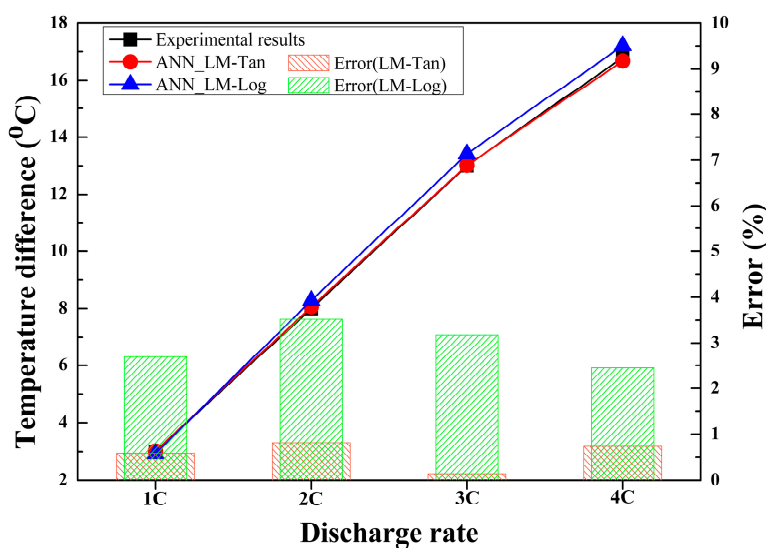


**Figure 10.** Variation in experimental and predicted temperature difference of batteries with change in discharge rate.

#### 4.1.3. Heat Transfer Coefficient

To assess the effectiveness of direct oil cooling for the battery module, the heat transfer coefficient was evaluated under various conditions of oil temperature, oil flow rate, and discharge rate, as shown in Figures 11–13. The convective heat transfer between batteries and oil improved when the oil temperature decreased and oil flow rate increased. Therefore, the lower battery temperature at the lower oil temperature and higher oil flow rate indicated a maximum heat transfer coefficient. The maximum heat transfer coefficients of  $3908.83 \text{ W/m}^2\text{-K}$  and  $2374.92 \text{ W/m}^2\text{-K}$  were evaluated corresponding to  $15^\circ\text{C}$  oil temperature and  $1.0 \text{ L/min}$  oil flow rate, respectively. There was no significant difference in heat transfer coefficient with change in discharge rate; however, the higher discharge rate enabled the opportunity for increased convective heat transfer from battery to oil owing to higher heat generation compared to the lower discharge rate. The maximum heat transfer coefficient of  $2741.22 \text{ W/m}^2\text{-K}$  was observed at a discharge rate of 4C. Closer agreement between the actual and predicted heat transfer coefficients was observed for the ANN\_LM-Tan algorithm under conditions of oil temperature, oil flow rate, and discharge rate with corresponding lowest maximum errors of 0.93%, 0.94%, and 0.79%, respectively. The highest maximum errors of 4.14%, 4.73%, and 4.17% were observed between ANN\_LM-Log-predicted and actual heat transfer coefficients in the case of oil temperature, oil flow rate, and discharge rate, respectively.

#### 4.2. Electrical Performance

The discharge voltage was evaluated and predicted using the ANN model as the electrical performance of the batteries under various conditions of oil temperature, oil flow rate, and discharge rate. The voltage results were predicted in the form of time series over the discharge period of the batteries for changes in influential factors. However, it should be noted that the voltage at the end of discharge was the same; hence, to compare the experimental and predicted results of voltage under variations of oil temperature, oil flow rate, and discharge rate, the voltage results were considered at the same discharge capacity.

#### Voltage

The effect of oil temperature on the voltage of batteries is depicted in Figure 14. The presented voltage results are compared at the same discharge capacity. The operating temperature of a battery affects the electrochemical characteristics of the battery; therefore, a change in oil temperature has a significant impact on the voltage of a battery during the discharge condition. The lower oil temperature showed a decreased voltage value,

which increased as the oil temperature increased because the lower oil temperature had a higher heat transfer rate from the batteries, which raised the internal resistance of the batteries. A drop in surrounding temperature results in the enhancement of ohmic resistance, which degrades the voltage of a battery [48]. In addition, Lu et al. claimed that the ionic conductivities of the SEI layer, electrode, and electrolyte were minimum at low temperature, which generates a decreasing voltage trend for the battery [49]. The voltage of the batteries dropped from 12.181 V to 10.996 V when the oil temperature decreased from 35 °C to 15 °C. Furthermore, the predicted voltages from the ANN model with two algorithms are compared to the experimental results under various oil temperatures in Figure 14. The overall error combining training, validation, and testing was higher in the case of the ANN\_LM-Log algorithm compared to the ANN\_LM-Tan algorithm, as presented in Figure 4. Therefore, the voltage predicted by the ANN\_LM-Tan algorithm showed closer agreement with the experimental voltage at all oil temperatures compared to that by the ANN\_LM-Log algorithm. The maximum errors between the experimental and predicted voltages by the ANN\_LM-Tan and ANN\_LM-Log algorithms were 0.88% and 4.81%, respectively.

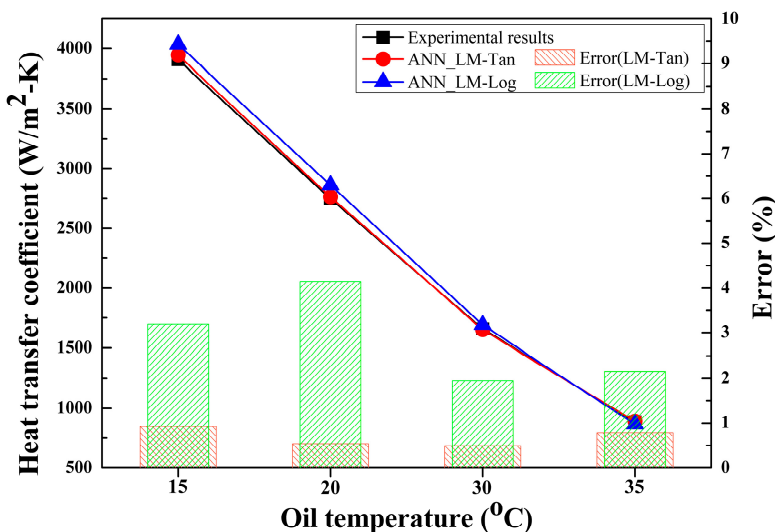


**Figure 11.** Variation in experimental and predicted heat transfer coefficient with change in oil temperature.

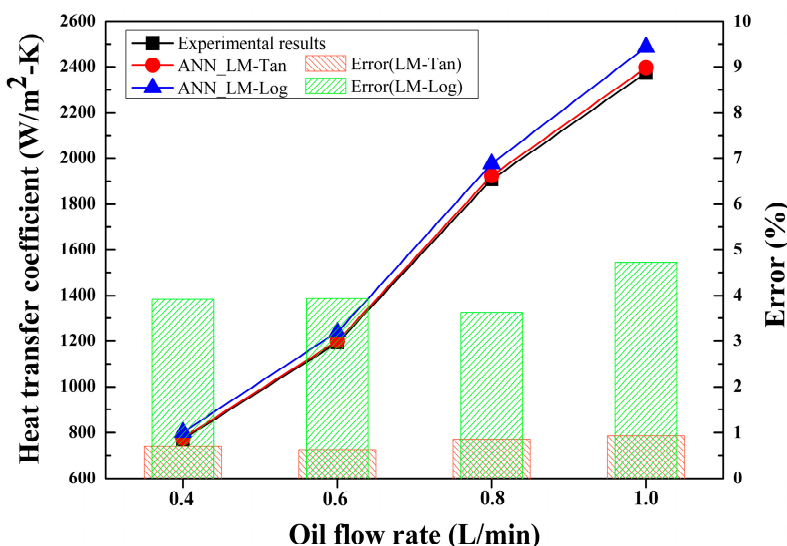


**Figure 12.** Variation in experimental and predicted heat transfer coefficient with change in oil flow rate.

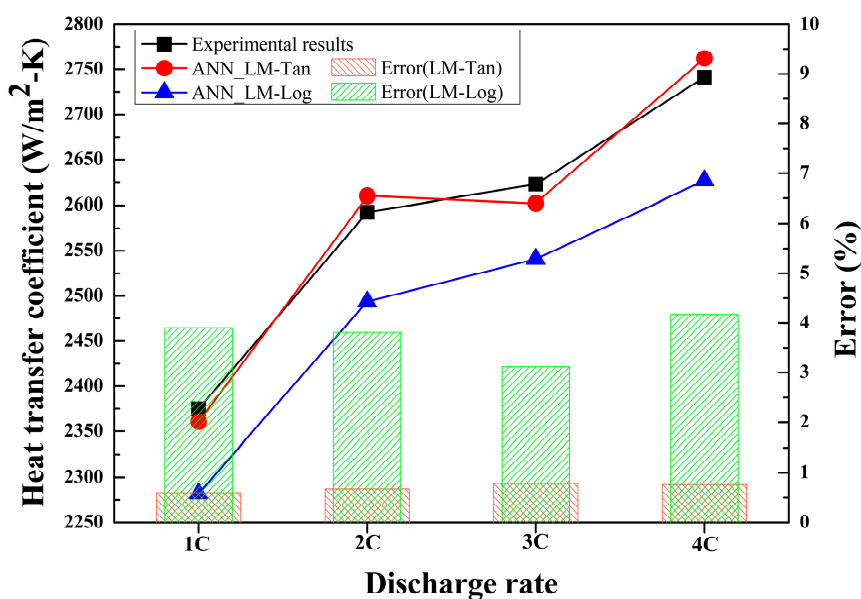


**Figure 13.** Variation in experimental and predicted heat transfer coefficient with change in discharge rate.

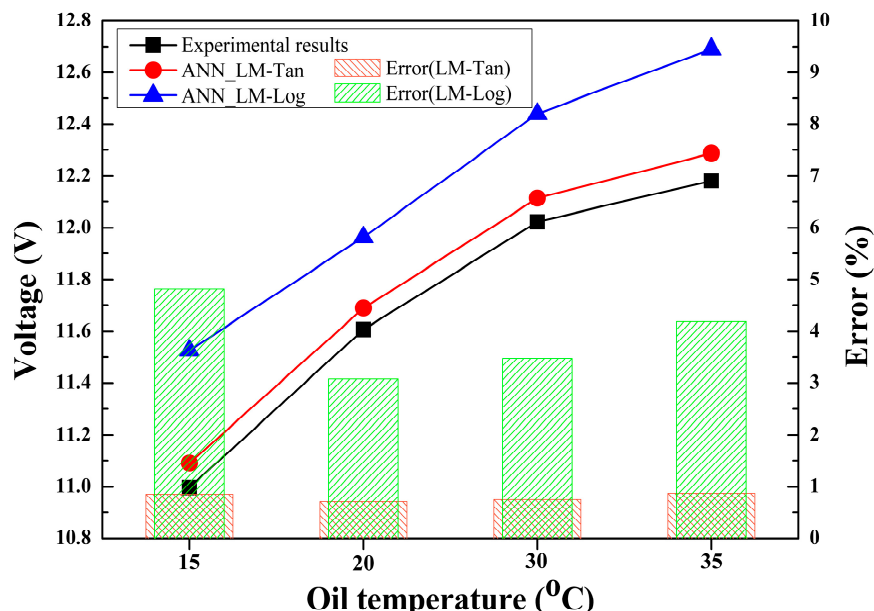


**Figure 14.** Variation in experimental and predicted voltage of batteries with change in oil temperature.

The effect of oil flow rate on experimental voltage and predicted voltage using both algorithms is depicted in Figure 15. An increase in oil flow rate indicates an improvement in battery cooling performance, which means the internal resistance of the battery increases with an increase in oil flow rate and thus a decrease in battery voltage during the discharge condition. Tong et al. also observed that the voltage of batteries dropped owing to a rise in the internal resistance of batteries when the battery cooling rate improved [50]. Therefore, the experimental and predicted voltage results showed a decreasing trend with an increase in oil flow rate. The voltage dropped from 11.113 V to 10.725 V with an increase in oil flow rate from 0.4 L/min to 1.0 L/min. The prediction accuracy for the ANN\_LM-Tan algorithm was higher compared to the ANN\_LM-Log algorithm with experimental voltages at each oil flow rate. The maximum prediction errors for the ANN\_LM-Tan and ANN\_LM-Log algorithms were 0.62% and 3.43%, respectively.

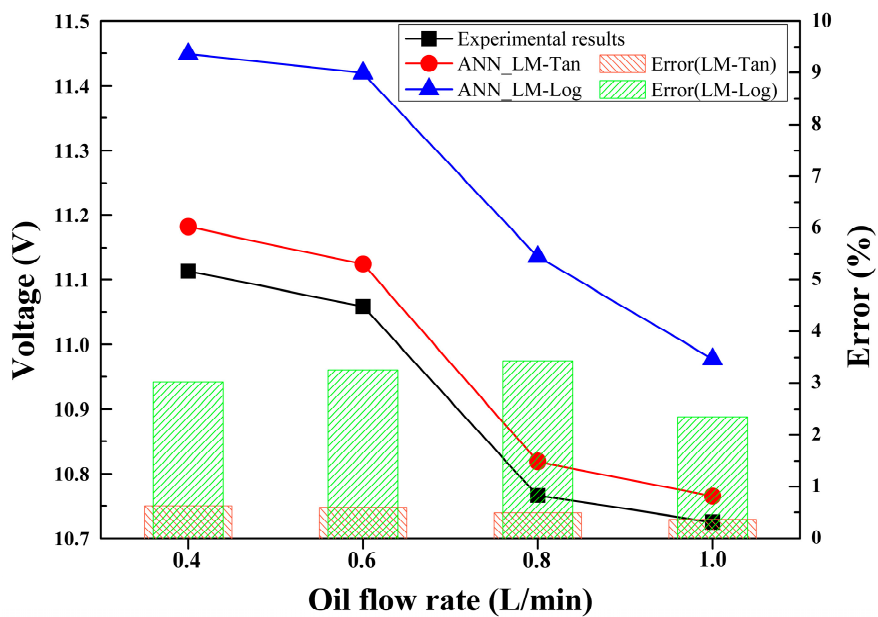


**Figure 15.** Variation in experimental and predicted voltage of batteries with change in oil flow rate.

The comparison of experimental and predicted voltages for different discharge conditions is shown in Figure 16. The voltage dropped rapidly as the discharge rate increased; therefore, at the same discharge capacity, the lower and higher discharge rates showed maximum and minimum voltages. The voltage dropped from 13.553 V to 10.725 V with an increase in discharge rate from 1C to 4C. The predicted voltages for both algorithms showed the same decreasing trend as the experimental voltage with the rise in discharge rate. However, the ANN\_LM-Tan algorithm was found to be an accurate model to predict closer voltages with corresponding experimental values compared to the ANN\_LM-Log algorithm. Considering all discharge rates, the maximum errors between the predicted voltages by the ANN\_LM-Tan and ANN\_LM-Log algorithms with the experimental voltage were 0.57% and 3.79%, respectively. As explained, the experimental and predicted results of the voltage were compared at the same discharge capacity of 8.136 Ah.

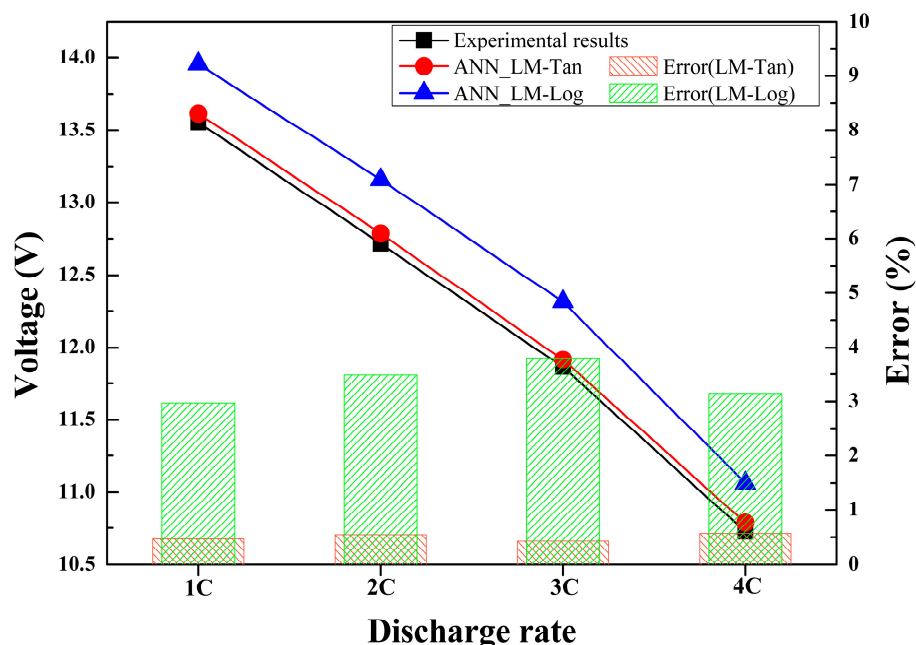


**Figure 16.** Variation in experimental and predicted voltage of batteries with change in discharge rate.

#### 4.3. Accuracy of Proposed ANN Model

The ANN\_LM-Tan algorithm depicted accurate predictions of all thermal and electrical performances under several conditions of oil temperature, oil flow rate, and discharge rate compared to the ANN\_LM-Log algorithm. Therefore, the ANN\_LM-Tan algorithm is suggested to replicate the various performances of battery modules with direct oil cooling under real operating conditions. Furthermore, to assure the accuracy and reliability of the suggested ANN model, the maximum temperature and voltage were predicted as thermal and electrical performances with change in discharge capacity and compared with the corresponding experimental results. The variations in experimental and ANN\_LM-Tan-predicted maximum temperature and voltage with discharge capacity are presented in Figure 17. This comparison is presented for an oil temperature of 30 °C, oil flow rate of 1.0 L/min, and discharge rate of 4C. For each condition of discharge capacity, the proposed ANN model depicted accurate replications of maximum temperature and voltage compared to the experimental data. The statistical parameters were calculated for the comparison, as presented in Figure 17, to quantify the accuracy of the predicted thermal and electrical performances. The calculated  $R^2$  and COV were 0.9998 and 1.55, respectively, in the case of maximum temperature, and 0.9997 and 1.66, respectively, in the case of voltage, indicating the reliability of the proposed ANN model to accurately mimic the actual condition data.

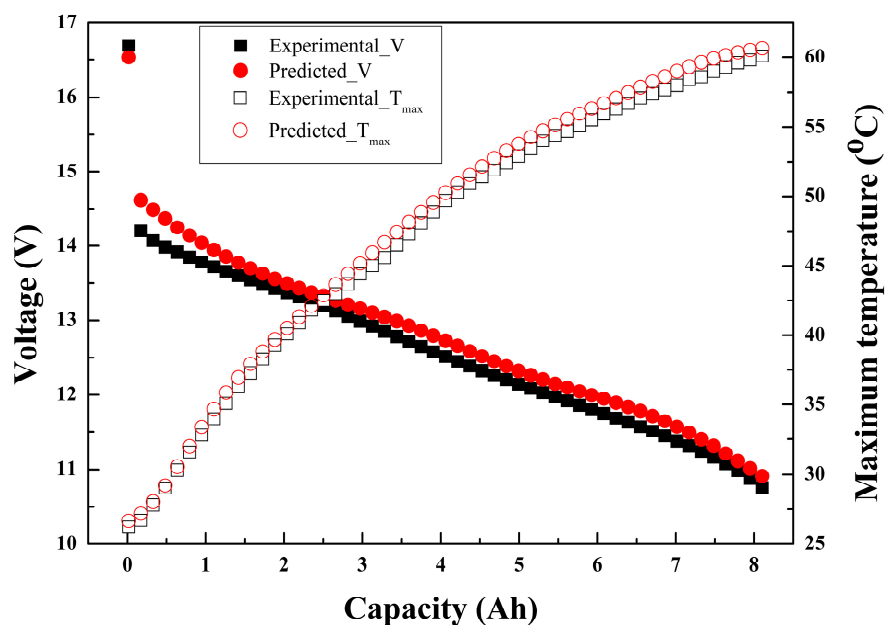


**Figure 17.** Variations in experimental and ANN\_LM-Tan-predicted maximum temperature and voltage with discharge capacity.

The development of an accurate neural network model enables replication of the performance of a battery with direct oil cooling under realistic operating conditions with minimal errors. The proposed neural network model could be used to generate a database relating the influential parameters and performance of batteries with direct oil cooling. Thus, several efforts in the development of prototypes could be minimized to fabricate a final-stage direct oil cooling system using the generated comprehensive reference database.

#### 5. Conclusions

The thermal and electrical performances of a battery module with direct oil cooling were experimentally evaluated and predicted using neural network models under several operating conditions. The following key findings are listed from the conducted present work.

- (a) The thermal performance in terms of maximum temperature, temperature difference, and heat transfer coefficient improves with a decrease in oil temperature. The lower maximum temperature and temperature difference of 44.6 °C and 6.9 °C, respectively, and higher heat transfer coefficient of 3908.83 W/m<sup>2</sup>-K were evaluated at a lower oil inlet temperature of 15 °C. The electrical performance in terms of voltage drops with a decrease in oil temperature, such that oil temperatures of 15 °C and 35 °C showed voltages of 10.996 V and 12.181 V, respectively.
- (b) An increase in oil flow rate reduces the maximum temperature, temperature difference, and voltage, whereas the heat transfer coefficient is enhanced. With an increase in oil flow rate from 0.4 L/min to 1.0 L/min, drops of 18.2 °C, 9.4 °C, and 0.388 V and an improvement of 1602.78 W/m<sup>2</sup>-K were observed in the maximum temperature, temperature difference, voltage, and heat transfer coefficient, respectively.
- (c) The maximum temperature and temperature difference increased by 27.8 °C and 13.8 °C, respectively, and the voltage dropped by 2.828 V with an increment in discharge rate from 1C to 4C. The maximum heat transfer coefficient of 2741.22 W/m<sup>2</sup>-K was evaluated at a higher discharge rate of 4C.
- (d) The ANN\_LM-Tan and ANN\_LM-Log algorithms showed maximum errors of 0.97% and 4.30% in the case of maximum temperature, 0.96% and 4.86% in the case of temperature difference, 0.94% and 4.73% in the case of heat transfer coefficient, and 0.88% and 4.81% in the case of voltage, respectively, considering all conditions of oil temperature, oil flow rate, and discharge rate. The prediction accuracy of the ANN\_LM-Tan algorithm was superior compared to the ANN\_LM-Log algorithm for all thermal and electrical performances under the considered operating conditions.
- (e) The ANN\_LM-Tan algorithm is recommended as the best neural network model to generate data of thermal and electrical performances under influential conditions for batteries with direct oil cooling. The reliability of the best neural network model was further established by predicting the maximum temperature and voltage for various discharge capacities, reflecting a maximum R<sup>2</sup> and COV of 0.99 and 1.66, respectively.
- (f) The proposed prediction model and prediction database could guide mapping the relationship between operating conditions and performance, which could be utilized to design and fabricate a direct liquid cooling system for high energy density batteries in electric vehicles. In future, tests will be conducted to develop prediction models for a battery module with direct oil cooling under fast charging and discharging conditions to assure the safety and reliability of the proposed next-generation battery thermal management technique.

**Author Contributions:** Conceptualization, K.S.G. and M.-Y.L.; methodology, K.S.G.; software, K.S.G.; formal analysis, K.S.G. and J.-W.H.; investigation, K.S.G. and S.-G.H.; resources, K.S.G. and M.-Y.L.; data curation, K.S.G. and S.-G.H.; writing—original draft preparation, K.S.G.; writing—review and editing, K.S.G. and M.-Y.L.; visualization, K.S.G., J.-W.H. and S.-G.H.; supervision, M.-Y.L.; project administration, M.-Y.L.; funding acquisition, M.-Y.L. All authors have read and agreed to the published version of the manuscript.

**Funding:** This work was supported by the Dong-A University research fund.

**Data Availability Statement:** The data presented in this study are available upon request to the corresponding author. The data are not publicly available due to privacy.

**Conflicts of Interest:** The authors declare no conflict of interest.

## References

1. Alanazi, F. Electric Vehicles: Benefits, Challenges, and Potential Solutions for Widespread Adaptation. *Appl. Sci.* **2023**, *13*, 6016. [[CrossRef](#)]
2. Stoma, M.; Dudziak, A. Future Challenges of the Electric Vehicle Market Perceived by Individual Drivers from Eastern Poland. *Energies* **2023**, *16*, 7212. [[CrossRef](#)]
3. Fresia, M.; Bracco, S. Electric Vehicle Fleet Management for a Prosumer Building with Renewable Generation. *Energies* **2023**, *16*, 7213. [[CrossRef](#)]

4. Ramraj, R.; Pashajavid, E.; Alahakoon, S.; Jayasinghe, S. Quality of Service and Associated Communication Infrastructure for Electric Vehicles. *Energies* **2023**, *16*, 7170. [[CrossRef](#)]
5. Liu, H.; Wei, Z.; He, W.; Zhao, J. Thermal issues about Li-ion batteries and recent progress in battery thermal management systems: A review. *Energy Convers. Manag.* **2017**, *150*, 304–330. [[CrossRef](#)]
6. Wilberforce, T.; El-Hassan, Z.; Khatib, F.N.; Al Makky, A.; Baroutaji, A.; Carton, J.G.; Olabi, A.G. Developments of electric cars and fuel cell hydrogen electric cars. *Int. J. Hydrot. Energy* **2017**, *42*, 25695–25734. [[CrossRef](#)]
7. Kumar, M.; Panda, K.P.; Naayagi, R.T.; Thakur, R.; Panda, G. Comprehensive Review of Electric Vehicle Technology and Its Impacts: Detailed Investigation of Charging Infrastructure, Power Management, and Control Techniques. *Appl. Sci.* **2023**, *13*, 8919. [[CrossRef](#)]
8. Dan, D.; Zhao, Y.; Wei, M.; Wang, X. Review of Thermal Management Technology for Electric Vehicles. *Energies* **2023**, *16*, 4693. [[CrossRef](#)]
9. Irfan, M.; Deilami, S.; Huang, S.; Veettil, B.P. Rooftop Solar and Electric Vehicle Integration for Smart, Sustainable Homes: A Comprehensive Review. *Energies* **2023**, *16*, 7248. [[CrossRef](#)]
10. Liu, H.; Xiao, Q.; Jin, Y.; Mu, Y.; Meng, J.; Zhang, T.; Jia, H.; Teodorescu, R. Improved LightGBM-Based Framework for Electric Vehicle Lithium-Ion Battery Remaining Useful Life Prediction Using Multi Health Indicators. *Symmetry* **2022**, *14*, 1584. [[CrossRef](#)]
11. Lu, L.; Han, X.; Li, J.; Hua, J.; Ouyang, M. A review on the key issues for lithium-ion battery management in electric vehicles. *J. Power Sources* **2013**, *226*, 272–288. [[CrossRef](#)]
12. Liu, Z.; Huang, J.; Cao, M.; Jiang, G.; Yan, Q.; Hu, J. Experimental study on the thermal management of batteries based on the coupling of composite phase change materials and liquid cooling. *Appl. Therm. Eng.* **2021**, *185*, 116415. [[CrossRef](#)]
13. Huang, Y.; Wei, C.; Fang, Y. Numerical investigation on optimal design of battery cooling plate for uneven heat generation conditions in electric vehicles. *Appl. Therm. Eng.* **2022**, *211*, 118476. [[CrossRef](#)]
14. Behi, H.; Karimi, D.; Behi, M.; Ghanbarpour, M.; Jaguemont, J.; Sokkeh, M.A.; Gandoman, F.H.; Berecibar, M.; Van Mierlo, J. A new concept of thermal management system in Li-ion battery using air cooling and heat pipe for electric vehicles. *Appl. Therm. Eng.* **2020**, *174*, 115280. [[CrossRef](#)]
15. Zhang, X.; Li, Z.; Luo, L.; Fan, Y.; Du, Z. A review on thermal management of lithium-ion batteries for electric vehicles. *Energy* **2022**, *238*, 121652. [[CrossRef](#)]
16. Jiaqiang, E.; Yi, F.; Li, W.; Zhang, B.; Zuo, H.; Wei, K.; Chen, J.; Zhu, H.; Zhu, H.; Deng, Y. Effect analysis on heat dissipation performance enhancement of a lithium-ion-battery pack with heat pipe for central and southern regions in China. *Energy* **2021**, *226*, 120336.
17. Panchal, S.; Khasow, R.; Dincer, I.; Agelin-Chaab, M.; Fraser, R.; Fowler, M. Thermal design and simulation of mini-channel cold plate for water cooled large sized prismatic lithium-ion battery. *Appl. Therm. Eng.* **2017**, *122*, 80–90. [[CrossRef](#)]
18. Akbarzadeh, M.; Kalogiannis, T.; Jaguemont, J.; Jin, L.; Behi, H.; Karimi, D.; Beheshti, H.; Van Mierlo, J.; Berecibar, M. A comparative study between air cooling and liquid cooling thermal management systems for a high-energy lithium-ion battery module. *Appl. Therm. Eng.* **2021**, *198*, 117503. [[CrossRef](#)]
19. Tan, X.; Lyu, P.; Fan, Y.; Rao, J.; Ouyang, K. Numerical investigation of the direct liquid cooling of a fast-charging lithium-ion battery pack in hydrofluoroether. *Appl. Therm. Eng.* **2021**, *196*, 117279. [[CrossRef](#)]
20. Roe, C.; Feng, X.; White, G.; Li, R.; Wang, H.; Rui, X.; Li, C.; Zhang, F.; Null, V.; Parkes, M.; et al. Immersion cooling for lithium-ion batteries—A review. *J. Power Sources* **2022**, *525*, 231094. [[CrossRef](#)]
21. Wu, S.; Lao, L.; Wu, L.; Liu, L.; Lin, C.; Zhang, Q. Effect analysis on integration efficiency and safety performance of a battery thermal management system based on direct contact liquid cooling. *Appl. Therm. Eng.* **2022**, *201*, 117788. [[CrossRef](#)]
22. Li, Y.; Zhou, Z.; Hu, L.; Bai, M.; Gao, L.; Li, Y.; Liu, X.; Li, Y.; Song, Y. Experimental studies of liquid immersion cooling for 18650 lithium-ion battery under different discharging conditions. *Case Stud. Therm. Eng.* **2022**, *34*, 102034. [[CrossRef](#)]
23. Patil, M.S.; Seo, J.H.; Lee, M.Y. A novel dielectric fluid immersion cooling technology for Li-ion battery thermal management. *Energy Convers. Manag.* **2021**, *229*, 113715. [[CrossRef](#)]
24. Sundin, D.W.; Sponholtz, S. Thermal management of Li-ion batteries with single-phase liquid immersion cooling. *IEEE Open J. Veh. Technol.* **2020**, *1*, 82–92. [[CrossRef](#)]
25. Zhou, H.; Dai, C.; Liu, Y.; Fu, X.; Du, Y. Experimental investigation of battery thermal management and safety with heat pipe and immersion phase change liquid. *J. Power Sources* **2020**, *473*, 228545. [[CrossRef](#)]
26. Dubey, P.; Pulugundla, G.; Srouji, A.K. Direct comparison of immersion and cold-plate based cooling for automotive Li-ion battery modules. *Energies* **2021**, *14*, 1259. [[CrossRef](#)]
27. Mazzeo, D.; Herdem, M.S.; Matera, N.; Bonini, M.; Wen, J.Z.; Nathwani, J.; Oliveti, G. Artificial intelligence application for the performance prediction of a clean energy community. *Energy* **2021**, *232*, 120999. [[CrossRef](#)]
28. Pang, Z.; Niu, F.; O'Neill, Z. Solar radiation prediction using recurrent neural network and artificial neural network: A case study with comparisons. *Renew. Energy* **2020**, *156*, 279–289. [[CrossRef](#)]
29. Panchal, S.; Dincer, I.; Agelin-Chaab, M.; Fraser, R.; Fowler, M. Design and simulation of a lithium-ion battery at large C-rates and varying boundary conditions through heat flux distributions. *Measurement* **2018**, *116*, 382–390. [[CrossRef](#)]
30. Wang, Q.K.; He, Y.J.; Shen, J.N.; Ma, Z.F.; Zhong, G.B. A unified modeling framework for lithium-ion batteries: An artificial neural network based thermal coupled equivalent circuit model approach. *Energy* **2017**, *138*, 118–132. [[CrossRef](#)]

31. Feng, F.; Teng, S.; Liu, K.; Xie, J.; Xie, Y.; Liu, B.; Li, K. Co-estimation of lithium-ion battery state of charge and state of temperature based on a hybrid electrochemical-thermal-neural-network model. *J. Power Sources* **2020**, *455*, 227935. [[CrossRef](#)]
32. Xie, Y.; He, X.J.; Hu, X.S.; Li, W.; Zhang, Y.J.; Liu, B.; Sun, Y.T. An improved resistance-based thermal model for a pouch lithium-ion battery considering heat generation of posts. *Appl. Therm. Eng.* **2020**, *164*, 114455. [[CrossRef](#)]
33. Arora, S.; Shen, W.; Kapoor, A. Neural network based computational model for estimation of heat generation in LiFePO<sub>4</sub> pouch cells of different nominal capacities. *Comput. Chem. Eng.* **2017**, *101*, 81–94. [[CrossRef](#)]
34. Liu, J.; Tavakoli, F.; Sajadi, S.M.; Mahmoud, M.Z.; Heidarshenas, B.; Aybar, H. Numerical evaluation and artificial neural network modeling of the effect of oval PCM compartment dimensions around a triple lithium-ion battery pack despite forced airflow. *Eng. Anal. Bound. Elem.* **2022**, *142*, 71–92. [[CrossRef](#)]
35. Jalilantabar, F.; Mamat, R.; Kumarasamy, S. Prediction of lithium-ion battery temperature in different operating conditions equipped with passive battery thermal management system by artificial neural networks. *Mater. Today Proc.* **2022**, *48*, 1796–1804. [[CrossRef](#)]
36. James, A.; Srinivas, M.; Mohanraj, M.; Raj, A.K.; Jayaraj, S. Experimental studies on photovoltaic-thermal heat pump water heaters using variable frequency drive compressors. *Sustain. Energy Technol. Assess.* **2021**, *45*, 101152. [[CrossRef](#)]
37. Holman, J.P. *Experimental Methods for Engineers*, 8th ed.; McGraw Hill Publisher: New York, NY, USA, 2021.
38. Raj, A.K.; Srinivas, M.; Jayaraj, S. A cost-effective method to improve the performance of solar air heaters using discrete macro-encapsulated PCM capsules for drying applications. *Appl. Therm. Eng.* **2019**, *146*, 910–920. [[CrossRef](#)]
39. Han, J.W.; Garud, K.S.; Kang, E.H.; Lee, M.Y. Numerical Study on Heat Transfer Characteristics of Dielectric Fluid Immersion Cooling with Fin Structures for Lithium-Ion Batteries. *Symmetry* **2022**, *15*, 92. [[CrossRef](#)]
40. Han, J.W.; Garud, K.S.; Hwang, S.G.; Lee, M.Y. Experimental Study on Dielectric Fluid Immersion Cooling for Thermal Management of Lithium-Ion Battery. *Symmetry* **2022**, *14*, 2126. [[CrossRef](#)]
41. Maduabuchi, C. Thermo-mechanical optimization of thermoelectric generators using deep learning artificial intelligence algorithms fed with verified finite element simulation data. *Appl. Energy* **2022**, *315*, 118943. [[CrossRef](#)]
42. Mohanraj, M.; Jayaraj, S.; Muraleedharan, C. Performance prediction of a direct expansion solar assisted heat pump using artificial neural networks. *Appl. Energy* **2009**, *86*, 1442–1449. [[CrossRef](#)]
43. Islam, K.T.; Raj, R.G.; Mujtaba, G. Recognition of traffic sign based on bag-of-words and artificial neural network. *Symmetry* **2017**, *9*, 138. [[CrossRef](#)]
44. Ullah, I.; Fayaz, M.; Kim, D. Improving accuracy of the Kalman filter algorithm in dynamic conditions using ANN-based learning module. *Symmetry* **2019**, *11*, 94. [[CrossRef](#)]
45. Moya-Rico, J.D.; Molina, A.E.; Belmonte, J.F.; Tendero, J.C.; Almendros-Ibanez, J.A. Characterization of a triple concentric-tube heat exchanger with corrugated tubes using Artificial Neural Networks (ANN). *Appl. Therm. Eng.* **2019**, *147*, 1036–1046. [[CrossRef](#)]
46. Kishore, R.A.; Mahajan, R.L.; Priya, S. Combinatory finite element and artificial neural network model for predicting performance of thermoelectric generator. *Energies* **2018**, *11*, 2216. [[CrossRef](#)]
47. Gunasekar, N.; Mohanraj, M.; Velmurugan, V. Artificial neural network modeling of a photovoltaic-thermal evaporator of solar assisted heat pumps. *Energy* **2015**, *93*, 908–922. [[CrossRef](#)]
48. Wu, H.; Zhang, X.; Cao, R.; Yang, C. An investigation on electrical and thermal characteristics of cylindrical lithium-ion batteries at low temperatures. *Energy* **2021**, *225*, 120223. [[CrossRef](#)]
49. Lu, Z.; Yu, X.L.; Wei, L.C.; Cao, F.; Zhang, L.Y.; Meng, X.Z.; Jin, L.W. A comprehensive experimental study on temperature-dependent performance of lithium-ion battery. *Appl. Therm. Eng.* **2019**, *158*, 113800. [[CrossRef](#)]
50. Tong, W.; Somasundaram, K.; Birgersson, E.; Mujumdar, A.S.; Yap, C. Numerical investigation of water cooling for a lithium-ion bipolar battery pack. *Int. J. Therm. Sci.* **2015**, *94*, 259–269. [[CrossRef](#)]

**Disclaimer/Publisher's Note:** The statements, opinions and data contained in all publications are solely those of the individual author(s) and contributor(s) and not of MDPI and/or the editor(s). MDPI and/or the editor(s) disclaim responsibility for any injury to people or property resulting from any ideas, methods, instructions or products referred to in the content.